DOI: 10.1002/chem.201100090

Nanoconfinement and Catalytic Dehydrogenation of Ammonia Borane by Magnesium-Metal–Organic-Framework-74

Srinivas Gadipelli,*[a, b] Jamie Ford,[a, b] Wei Zhou,[a, c] Hui Wu,[a, c] Terrence J. Udovic,[a] and Taner Yildirim*[a, b]

Ammonia borane (NH_3BH_3, AB) has recently received much attention as a promising hydrogen-storage medium among a very large number of candidate materials because of its satisfactory air stability, relatively low molecular mass (30.7 $g\,mol^{-1}$), and remarkably high energy-storage densities (gravimetric and volumetric hydrogen capacities are 19.6 wt% and 140 $g\,L^{-1}$, respectively).[1–6] However, the direct use of pristine AB as a hydrogen energy carrier in on-board/fuel-cell applications is prevented by its very slow dehydrogenation kinetics below 100 °C and the concurrent release of detrimental volatile by-products such as ammonia, borazine, and diborane.[2,3] Many different methods have been adopted[1–7] to promote efficient H_2 generation from AB, including catalytic hydrolysis in aqueous solution,[8] ionic liquids,[9] organic solvents,[10] and thermodynamic modifications by formation of hybrid structures with transition metals,[2,8] alkali-, or alkaline-earth metal/hydrides,[11,12] or nanoconfined phases using porous scaffolds.[13–22] However, many of these methods rely on the usage of heavy metal catalysts, aqueous or nonaqueous solutions, and ionic liquids, all of which make the hydrogen density of the systems unacceptably low for practical applications.[3] Furthermore, the vigorous reactions, hygroscopic properties, and water solubility of borohydrides have negative impacts on the dehydrogenation performance and make it difficult to control the release of hydrogen. The other approach is made, in particular, nanocomposition of AB within porous scaffoldings.[2,16–22] However, systems still suffers one or more of the followings: either the nanocomposite is heavier or cannot prevent the generation of all the volatile by-products. Hence, more work needs to be done to explore the potential role that catalysts can play to further improve the controllable H_2-release kinetics under moderate conditions while at the same time preventing the generation of detrimental by-products.

Over the past few years, porous metal–organic frameworks (MOFs)[23] have emerged as promising multifaceted materials,[23–25] combining such functions as catalytic activity,[17,18,24] shape-selectivity,[23–25] templating,[14] and purification.[25] Crystalline MOF structures are composed of metal sites linked to organic ligands, yielding three-dimensional extended frameworks that often possess considerable porosity. In principle, the combination of nanoporosity and active metal sites in MOFs makes them potentially useful materials for promoting the decomposition of AB. However, until now, such a use of MOFs has been rare[17,18] and any future success would depend crucially on the particular choices of a suitable metal center, pore structure, and thermal stability. For instance, Li et al.[17] were the first to show that Y-based MOF as a solid state decomposition agent for AB. The main drawback of AB-Y-MOF is largely added weight due to the heavy Y metal. In addition, for the given very narrow pore structure of Y-MOF, as low as approximately 8 wt% of AB loading is achieved for the reported 1:1 mole ratio. Thus, it is highly desirable to have a light weight MOF with stable and suitable nanopore channels that can hold more than one AB molecule. Herein, we show that the porous Mg-MOF-74 (Mg_2(DOBDC), DOBDC = 2, 5-dioxido-1, 4-benzenedicarboxylate)[26–28] is a promising candidate for nanoconfinement and catalytic decomposition of AB for clean and efficient H_2 generation.

Mg-MOF-74 has a rigid framework, composed of one-dimensional (1D) hexagonal channels (Figure 1a) with a nominal diameter of approximately 12 Å running parallel to the DOBDC ligands.[26–28] In as-synthesized material, the Mg^{2+} cations are coordinated with five oxygen atoms from the DOBDC ligands and one oxygen atom from a terminal water molecule. However, upon heating under vacuum, the terminal water molecules can be easily removed, leading to unsaturated (open) Mg metal sites (decorated on the edges of the hexagonal pore channels) with an open pore structure of high surface area (> 1000 m^2g^{-1}).[26] The open Mg metal sites play a vital role in enhanced binding of various gas molecules (H_2, CH_4, C_2H_2, NO, etc.[26–28]) and successfully used to promote molecular separation.[25] Figure 1b represents AB confinement within the MOF pores as obtained

[a] Dr. S. Gadipelli, Dr. J. Ford, Dr. W. Zhou, Dr. H. Wu, Dr. T. J. Udovic, Dr. T. Yildirim
NIST Center for Neutron Research
Gaithersburg MD 20899-6102 (USA)
Fax: (+1) 301-921-9847
E-mail: taner@seas.upenn.edu
gsrini@seas.upenn.edu

[b] Dr. S. Gadipelli, Dr. J. Ford, Dr. T. Yildirim
Department of Materials Science and Engineering
University of Pennsylvania, Philadelphia PA, 19104 (USA)

[c] Dr. W. Zhou, Dr. H. Wu
Department of Materials Science and Engineering
University of Maryland, College Park MD, 20742 (USA)

Supporting information for this article is available on the WWW under http://dx.doi.org/10.1002/chem.201100090.

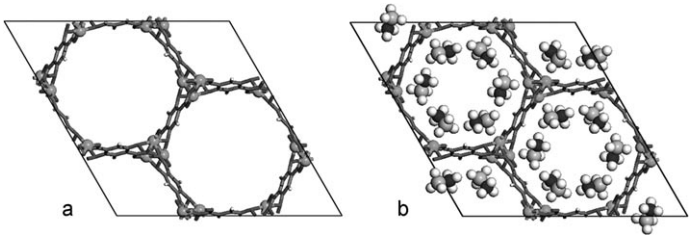

Figure 1. a) The framework structure of one-dimensional hexagonal shaped open pore channels of clean Mg-MOF-74. b) The confinement of AB within the pores.

from our first-principles structural optimization (see the Supporting Information) for a loading of one AB per Mg^{2+} cation (1:1 mole ratio). This corresponds to 18 AB molecules per hexagonal unit cell, equivalent to approximately 26 wt%, which is significantly larger than the approximately 8 wt% of AB loading in a Y-MOF system.[17]

The successful incorporation of AB into the nanopores of Mg-MOF (see the Supporting Information, for synthesis and experimental details) at different loading levels is demonstrated by powder X-ray diffraction (XRD) (Figure 2 and S1

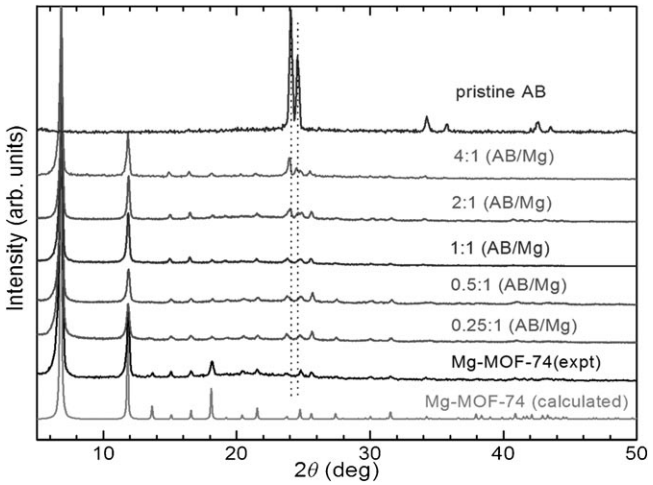

Figure 2. X-ray diffraction patterns of clean and AB-loaded Mg-MOF-74 and pristine AB. The dotted vertical lines represent the positions of pristine AB peaks, which only appear for 2:1 and 4:1 AB/Mg samples.

in the Supporting Information), nitrogen and hydrogen gas sorption measurements at 77 K (Figure S3 in the Supporting Information), and Fourier transform infrared (FTIR) spectroscopic analyses (Figure S4 in the Supporting Information). The XRD patterns of the AB-Mg-MOF system show no notable change in structural parameters, indicating that the framework structure retains its integrity upon AB infiltration. The disappearance of crystalline AB peaks at low loading as well as decreased MOF peak intensities, especially the first two reflections, suggests that AB is confined within the pores of MOF. In contrast, at high loading ($\geq$2:1 AB/Mg), the reappearance of characteristic AB diffraction peaks indicates the aggregation of excess bulk AB phase outside the saturated nanopore channels. Furthermore, the negligible N_2 and H_2 adsorption in the AB-Mg-MOF system compared to the clean MOF indicates complete pore filling by AB guest molecules. At low loading, the FTIR spectra exhibit no obvious difference between clean MOF and AB-loaded MOFs. The B–H modes associated with AB only appear at higher loadings.

Figure 3, S5, and S6 in the Supporting Information show the thermal decomposition behaviors of pristine AB and the AB-Mg-MOF system obtained using simultaneous thermog-

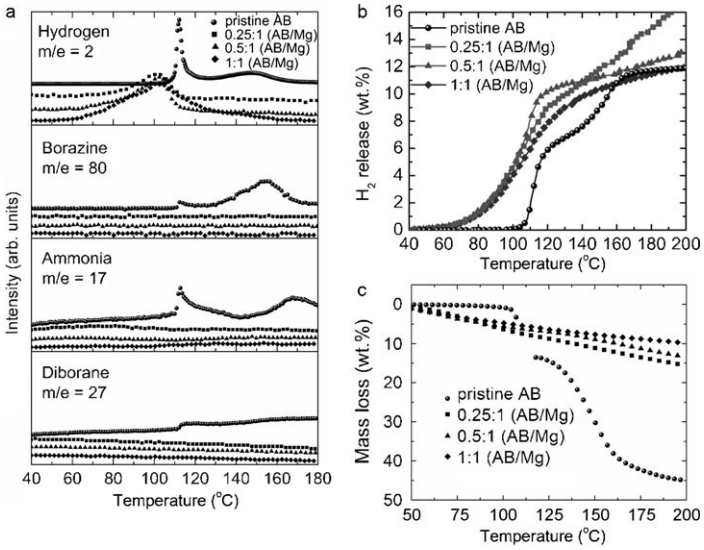

Figure 3. a) TG-MS, b) TPD, and c) TG results of AB-Mg-MOF-74 with different levels of AB loading in the MOF.

ravimetry, differential scanning calorimetry, and mass spectrometry (TG/DSC/MS), and independent volumetric temperature programmed desorption (TPD) analysis. As we are interested in improvements in hydrogen-release properties of the AB-MOF system compared to AB alone, the hydrogen contents from the volumetric desorptions are based on AB alone and not on the combined AB-MOF system. In this way, we get better idea about the improvements made between pristine AB and different AB loaded MOF systems. In agreement with previous studies,[2] pristine AB releases H_2 above 100 °C in a two-step process and the concurrent generation of volatile by-products of ammonia, borazine, and diborane is clearly observed. This qualitatively accounts for the TG result of the pristine AB, where a significantly larger mass loss (ca. 45%) than the expected value (ca. 13%) for H_2 release is observed. The prominent endothermic and exothermic peaks in DSC indicate that AB melts before it starts to decompose.

In contrast, the low loading AB-Mg-MOFs exhibit significant improvements in terms of both hydrogen release temperature and absence of unwanted by-products. The H_2 release temperature has decreased to $<$70 °C and the dehydrogenation is a single-step process, peaking at approximately

100 °C. The volumetric TPD estimates about 11 wt % of H_2 capacity at 120 °C compared to 6 wt % of H_2 capacity for pristine AB. The releases of 16 wt % at 200 °C is also very high compared to the approximately 12 wt % of H_2 from pristine AB. Most importantly, MS results show no signs of any detectable ammonia, borazine, or diborane during the thermal desorption process for temperatures up to 200 °C. The complete prevention of volatile by-products is also evident from TG results, in which the mass loss is considerably reduced compared to pristine AB. In addition, the TG mass loss of the AB-Mg-MOF system is in good agreement with the volumetrically obtained TPD results. The DSC (Figure S5 in the Supporting Information) results show largely reduced exothermicity without endothermic melting peaks, indicating the direct solid-state decomposition of the nanoconfined AB.

The dehydrogenation of heavily loaded AB-MOFs indicates the combined H_2 release from both nanoconfined AB and excess crystalline AB aggregates outside the saturated nanopores. Furthermore, the presence of the excess AB aggregates is clearly seen from the excess mass loss in TG, and the prominent endothermic/exothermic peaks in DSC that are similar to pristine AB. The TPD results indicate a bulk AB-like behavior. Interestingly, the system still exhibits greatly suppressed volatile by-products (Figure S6 in the Supporting Information). Thus, the observed changes in desorption behavior with AB loading further support the importance of nanoconfinement and AB interaction with the active metal-centers for promoting efficient, clean H_2 release.

The controlled H_2 release and dehydrogenation behavior for different AB loadings are further demonstrated by isothermal desorption kinetics measured at various temperatures. Figure 4 and S7 in the Supporting Information compare the dehydrogenation kinetics plots of pristine AB and the AB-Mg-MOFs. In agreement with the literature, the pristine AB exhibits very poor desorption kinetics and release only approximately 6 wt % of H_2 at temperatures just over 100 °C.[2,9] On the contrary, in the case of AB-Mg-MOF system H_2 release starts immediately without an induction period when temperatures are above 65 °C. The samples generate 10–12 wt % of clean H_2 in less than 20 minutes at temperatures slightly above 100 °C. When the temperature is below 100 °C, about 9 wt % of clean H_2 is generated within 25 min, 90 minutes, and 7 hours at 95 °C, 85 °C, and 75 °C, respectively. In any case, we note that the values are significantly greater than the maximum release of approximately 6 wt % of H_2 from the pristine AB between 85 °C and 125 °C. The 14 wt % of clean H_2 at 125 °C in 1 hour from our AB-MOF system represents a significant improvement, and it is also higher than the theoretically predicted approximately 13 wt % from pristine AB, which only occurs at temperatures above 200 °C.[2] Finally, we note that the hydrogen-release kinetics are also very sensitive to the level of AB-loading. At high loading, the kinetics are quite similar to the bulk-like AB (see Figure S7 in the Supporting Information), suggesting the importance of the AB–AB intermolecular interactions between nanoconfined and bulk phase AB.

To understand the desorption mechanism of AB-Mg-MOF system, the samples used in the thermal desorption studies were further studied with XRD (Figure S2 in the Supporting Information), FTIR (Figure S4 in the Supporting Information), gas adsorption analyses (Figure S3 in the Supporting Information), and inelastic neutron scattering (INS) (Figure 5). All the results demonstrate that the integrity of MOF structure did not change after the thermal desorption. In contrast to the IR spectra, for 1:1 AB/Mg sample, the clear AB phonon modes, albeit broad, are seen in INS spectrum (Figure 5). The INS spectrum of AB-Mg-MOF after thermal desorption at temperatures up to 200 °C is similar to that for the clean Mg-MOF, with slight differences due to the remaining residue of B and N complexes. Importantly, there is no obvious change in H_2 and N_2 adsorption properties between AB-Mg-MOF systems before and after thermal desorption (Figure S3 in the Supporting Information). Because H_2 adsorption is mainly due to the open Mg metal sites and N_2 is defined by open pore structure, the observed behaviors indicate that the open Mg metal sites and 1D nanopore channels are remain inaccessible even after thermal desorption. This suggests that the Mg sites and nanopores are occupied by remaining complexes made of B and

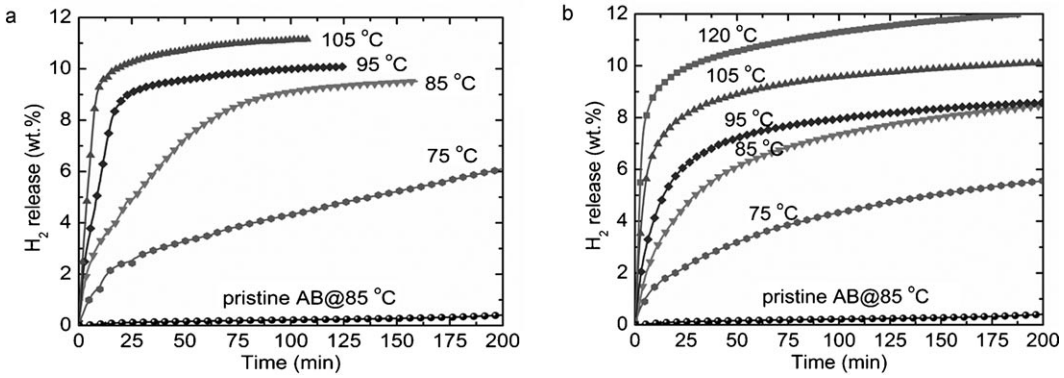

Figure 4. The isothermal H_2 desorption kinetics of AB-Mg-MOF-74 at different temperatures for AB/Mg mole ratios of a) 0.5 and b) 1.

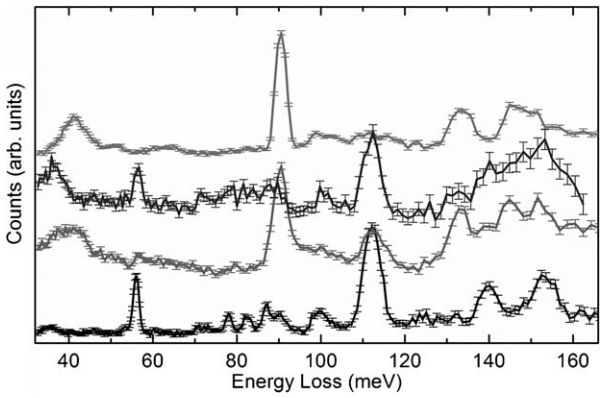

Figure 5. The inelastic neutron scattering spectra at 4 K of clean Mg-MOF-74 (bottom), AB-loaded Mg-MOF-74 (1:1 AB/Mg) before (2nd from bottom) and after (3rd from bottom) H_2 thermal desorption at temperatures up to 200 °C, and pristine AB (top).

N atoms after dehydrogenation. In fact, earlier it was shown that B interacts with O groups on the porous support due to the electropositive B in -BH_3 and electron donating O. Also the metallic catalyst is likely to interact with the -NH_3 group in AB.[2,16–22] This leads to greatly weakened N–B and B–H bonds, which could lead to improved desorption kinetics as well as reduction in dehydrogenation temperature. The interaction of Mg and the organic linker with N and B, also explains the suppression of ammonia, borazine and diborane for the samples with loading levels of up to 1:1 AB/Mg. The early hydrogen release from weakened B–H bonding is evidenced from the FTIR spectra at 105 °C (Figure S4 in the Supporting Information). After thermal desorption, a new IR mode near 1025 cm^{-1} appears in the FTIR spectra of the AB-loaded samples. We attribute this to the phonons of boron atoms trapped in the MOF pores that interact with the surrounding oxygen atoms.[29,30] XRD, FTIR, and INS spectra show no change in the MOF modes after thermal desorption, further assuring that the Mg-MOF-structure is stable and does not disintegrate with AB-loading. This is very different than many other MOFs that decompose with AB loading. In SI, we present results from two such MOFs (Ni-MOF-74 and HKUST-1). The XRD and TPD measurements shown in Figure S8–S10 in the Supporting Information clearly indicate that these MOFs disintegrate with AB-loading, even before thermal desorption. Hence, the AB-Mg-MOF system is unique and provides a novel way to generate clean hydrogen with fast kinetics from AB molecules. Our first-principles structure optimization and phonon calculations for both an isolated AB molecule and the AB-MOF system (see Figure S11 in the Supporting Information) indicates the shortened B–N bond length of approximately 0.03 Å compared to the isolated molecule. Consistent with these results, we also observe that several phonon energies soften as much as 10 meV, in agreement with the lower decomposition temperature with confinement. Furthermore, in addition to the surface interactions, the considerably increased surface area for the infiltrated AB due to limited nanoconfinement within the pore channels leads to enhanced kinetics. To support this, the heavily loaded AB-MOF system behaves like pristine AB in terms of dehydrogenation temperature as well as desorption kinetics due to increased AB–AB interactions and presence of bulk AB.

In summary, we showed that the nanoconfinement of AB molecules within the one-dimensional pores of Mg-MOF-74 improves the dehydrogenation kinetics significantly at temperatures <100 °C. More importantly, the AB-Mg-MOF-74 system offers clean hydrogen delivery by suppressing the detrimental by-products of ammonia, borazine and diborane. Furthermore, due to its high surface area, pore volume fraction, and low-mass elements, the Mg-MOF system can accommodate a large mass fraction up to approximately 26 wt.% of nanoconfined AB corresponding to a 1:1 AB/Mg molar ratio compared to approximately 8 wt.% AB in the Y-MOF[17] without much compromise in dehydrogenation temperature or kinetics behavior. Our systematic investigation shows that the dehydrogenation properties of the AB-Mg-MOF-74 system depend on the level of AB loading, thus indicating the importance of nanoconfinement and the significant role that Mg metal centers play. MOFs with other metals, such as Ni (in Ni-MOF-74) and Cu (in HKUST-1), disintegrate with AB loading and are not suitable for the nanoconfinement of AB molecules. Due to the large variety of MOF structures with different pore size/shape, metal types and coordination, it is quite possible that there are other MOFs with even better AB-loading capacity and with enhanced hydrogen release kinetics. One remaining issue is the regeneration of the MOFs after thermal desorption. Our future efforts will focus on solving this problem.

Experimental Section

Synthesis of Mg-MOF-74: Mg-MOF-74 was synthesized according to the reported procedure under solvothermal conditions in a mixture of dimethyl formamide (DMF)/ethanol/water at 125 °C.[26,28] To remove occluded DMF, the product was exchanged with methanol many times for several days. Then, the final activation of MOF to remove methanol and water molecules on the open metal sites was done by evacuation at 200 °C for 24 h under dynamic vacuum. The activation of MOF is essential prior to use of MOF for analysis of the pore structure or activity of the metal centers, and to remove terminal water molecules.

Synthesis of AB-Mg-MOF-74: The AB loaded Mg-MOFs were synthesized through a simple solution-blending process. AB (Sigma Aldrich, 97%)[31] was dissolved in anhydrous methanol (0.5 M) at room temperature in a glove bag. The required amount of activated MOF was then added to the solution and the mixture was stirred for 30 min at room temperature. The homogeneous solution was then dried under high vacuum at for 24 h to remove any methanol trapped in the pores and stored in a helium filled glove box.[17,18] Further handling of the samples for all the characterizations was done in a glove box.

Characterization: The powder XRD patterns were obtained on samples sealed in a glass capillary in the glove box on a Rigaku D/max-2200PC X-ray diffractometer with $Cu_{K\alpha}$ radiation. INS data were collected on the BT-4 Filter-Analyzer Neutron Spectrometer (FANS) with the Cu(220) monochromator at 4 K.[32] The N_2 sorption BET surface area measurements were performed on a Quantachrome Autosorb-1 at 77 K. The high-pressure H_2 sorption was obtained using a home-built Sievert apparatus.[33] The FTIR spectra were collected at room temperature using the

KBr-pellet method on the NEXUS 670 FT-IR spectrometer. The simultaneous TG/DSC/MS measurements were carried out on a TA Instruments Q600 simultaneous DSC/TGA combined with a Pfeiffer thermostar vacuum quadrupole mass spectrometer at a ramping rate of 2 °C min^{-1} under N_2 atmosphere. The volumetric TPD (with heating rate of 2 °C min^{-1}) and isothermal dehydrogenation kinetics measurements were performed using a carefully calibrated Sievert apparatus.

Acknowledgements

This work was supported by DOE BES Grant No. DE-FG02–08ER46522.

Keywords: ammonia borane · dehydrogenation · kinetics · metal–organic frameworks · nanoconfinement

[1] N. C. Smythe, J. C. Gordon, *Eur. J. Inorg. Chem.* **2010**, 509–521.
[2] A. Staubitz, A. P. M. Robertson, I. Manners, *Chem. Rev.* **2010**, *110*, 4079–4124.
[3] J. Yang, A. Sudik, C. Wolverton, D. J. Siegel, *Chem. Soc. Rev.* **2010**, *39*, 656–675.
[4] A. Staubitz, A. P. M. Robertson, M. E. Sloan, I. Manners, *Chem. Rev.* **2010**, *110*, 4023–4078.
[5] C. W. Hamilton, R. T. Baker, A. Staubitz, I. Manners, *Chem. Soc. Rev.* **2009**, *38*, 279–293.
[6] F. H. Stephens, V. Pons, R. T. Baker, *Dalton Trans.* **2007**, 2613–2626.
[7] H. Wu, W. Zhou, F. E. Pinkerton, M. S. Meyer, G. Srinivas, T. Yildirim, T. J. Udovic, J. J. Rush, *J. Mater. Chem.* **2010**, *20*, 6550–6556.
[8] F. Y. Cheng, H. Ma, Y. M. Li, J. Chen, *Inorg. Chem.* **2007**, *46*, 788–794.
[9] M. E. Bluhm, M. G. Bradley, R. Butterick, U. Kusari, L. G. Sneddon, *J. Am. Chem. Soc.* **2006**, *128*, 7748–7749.
[10] M. C. Denney, V. Pons, T. J. Hebden, D. M. Heinekey, K. I. Goldberg, *J. Am. Chem. Soc.* **2006**, *128*, 12048–12049.
[11] J.-H. Luo, X.-D. Kang, P. Wang, *J. Phys. Chem. C* **2010**, *114*, 10606–10611.
[12] N. Brun, R. Janot, C. Sanchez, H. Deleuze, C. Gervais, M. Morcrette, R. Backov, *Energy Environ. Sci.* **2010**, *3*, 824.
[13] T. K. Nielsen, U. Bösenberg, R. Gosalawit, M. Dornheim, Y. Cerenius, F. Besenbacher, T. R. Jensen, *ACS Nano* **2010**, *4*, 3903–3908.
[14] R. K. Bhakta, J. L. Herberg, B. Jacobs, A. Highley, R. Behrens Jr. , N. W. Ockwig, J. A. Greathouse, M. D. Allendorf, *J. Am. Chem. Soc.* **2009**, *131*, 13198–13199.
[15] X. D. Kang, Z. Z. Fang, L. Y. Kong, H. M. Cheng, X. D. Yao, G. Q. Lu, P. Wang, *Adv. Mater.* **2008**, *20*, 2756–2759.
[16] J. Zhao, J. Shi, X. Zhang, F. Cheng, J. Liang, Z. Tao, J. Chen, *Adv. Mater.* **2010**, *22*, 394–397.
[17] Z. Li, G. Zhu, G. Lu, S. Qiu, X. Yao, *J. Am. Chem. Soc.* **2010**, *132*, 1490–1491.
[18] Y. Li, P. Song, J. Zheng, X. Li, *Chem. Eur. J.* **2010**, *16*, 10887–10892.
[19] H. Kim, A. Karkamkar, T. Autrey, P. Chupas, T. Proffen, *J. Am. Chem. Soc.* **2009**, *131*, 13749–13755.
[20] S. Sepehri, B. B. García, G. Cao, *Eur. J. Inorg. Chem.* **2009**, 599–603.
[21] L. Li, X. Yao, C. Sun, A. Du, L. Cheng, Z. Zhu, C. Yu, J. Zou, S. C. Smith, P. Wang, H.-M. Cheng, R. L. Frost, G. Q. Lu, *Adv. Funct. Mater.* **2009**, *19*, 265–271.
[22] A. Gutowska, L. Li, Y. Shin, C. M. Wang, X. S. Li, J. C. Linehan, R. S. Smith, B. D. Kay, B. Schmid, W. Shaw, M. Gutowski, T. Autrey, *Angew. Chem.* **2005**, *117*, 3644–3648; *Angew. Chem. Int. Ed.* **2005**, *44*, 3578–3582.
[23] G. Férey, *Chem. Soc. Rev.* **2008**, *37*, 191–214.
[24] A. Corma, H. García, F. X. Llabrés i Xamena, *Chem. Rev.* **2010**, *110*, 4606–4655.
[25] J.-R. Li, R. J. Kuppler, H.-C. Zhou, *Chem. Soc. Rev.* **2009**, *38*, 1477–1504.
[26] S. R. Caskey, A. G. Wong-Foy, A. J. Matzger, *J. Am. Chem. Soc.* **2008**, *130*, 10870–10871.
[27] H. Wu, J. M. Simmons, G. Srinivas, W. Zhou, T. Yildirim, *J. Phys. Chem. Lett.* **2010**, *1*, 1946–1951.
[28] W. Zhou, H. Wu, T. Yildirim, *J. Am. Chem. Soc.* **2008**, *130*, 15268–15269.
[29] U. B. Demirci, S. Bernard, R. Chiriac, F. Toche, P. Miele, *J. Power Sources* **2011**, *196*, 279–286.
[30] L. Jun, Z. Shuping, G. Shiyang, *Spectrochim. Acta Part A* **1995**, *51*, 519–532.
[31] Certain trade names and company products are mentioned in this paper to adequately specify the experimental procedure and equipment used. In no case does this imply recommendation or endorsement by NIST, nor does it imply that the products are necessarily the best available for this purpose.
[32] T. J. Udovic, C. M. Brown, J. B. Leão, P. C. Brand, R. D. Jiggetts, R. Zeitoun, T. A. Pierce, I. Peral, J. R. D. Copley, Q. Huang, D. A. Neumann, and R. J. Fields, *Nucl. Instrum. Methods Phys. Res. Sect. A* **2008**, *588*, 406–413.
[33] W. Zhou, H. Wu, M. R. Hartman, T. Yildirim, *J. Phys. Chem. C* **2007**, *111*, 16131–16137.

Received: January 10, 2011
Published online: April 20, 2011

